Energy bands in graphene: Comparison between the tight-binding model and *ab initio* calculations

E. Kogan,[1,*] V. U. Nazarov,[2,†] V. M. Silkin,[3,‡] and M. Kaveh[1,§]

[1]*Jack and Pearl Resnick Institute, Department of Physics, Bar-Ilan University, Ramat-Gan 52900, Israel*

[2]*Research Center for Applied Sciences, Academia Sinica, Taipei 11529, Taiwan*

[3]*Donostia International Physics Center (DIPC), Paseo de Manuel Lardizabal 4, E-20018 San Sebastian/Donostia, Spain; Departamento de Física de Materiales, Facultad de Ciencias Químicas, UPV/EHU, Apartado 1072, E-20080 San Sebastian/Donostia, Spain; and IKERBASQUE, Basque Foundation for Science, 48011 Bilbao, Spain*

(Received 17 December 2013; revised manuscript received 10 April 2014; published 29 April 2014)

We compare the classification of the electron bands in graphene, obtained by group theory algebra in the framework of a tight-binding model (TBM), with that calculated in a density-functional-theory (DFT) framework. Identification in the DFT band structure of all eight energy bands (four valence and four conduction bands) corresponding to the TBM-derived energy bands is performed and the corresponding analysis is presented. The four occupied (three σ-like and one π-like) and three unoccupied (two σ-like and one π-like) bands given by the DFT closely correspond to those predicted by the TBM, both by their symmetry and their dispersion law. However, the two lowest lying at the Γ-point unoccupied bands (one of them of a σ-like type and the other of a π-like one), are not of the TBM type. According to both their symmetry and the electron density these bands are plane waves orthogonal to the TBM valence bands; dispersion of these states can be determined unambiguously up to the Brillouin zone borders. On the other hand, the fourth unoccupied band given by the TBM can be identified among those given by the DFT band calculations; it is situated rather high with respect to energy. The interaction of this band with the free-electron states is so strong that it exists only in part of the k space.

DOI: 10.1103/PhysRevB.89.165430 PACS number(s): 73.22.Pr

I. INTRODUCTION

In the course of the study of graphite and a graphite monolayer, called graphene, understanding of the symmetries of the electron dispersion law in graphene was of crucial importance. Actually, the symmetry classification of the energy bands in graphene (or "two-dimensional graphite") was presented nearly 60 years ago by Lomer in his seminal paper [1]. Later the subject was analyzed by Slonczewski and Weiss [2], Dresselhaus and Dresselhaus [3], and Bassani and Parravicini [4]. Some recent approaches to the problem are presented in Refs. [5–9].

In the vast majority of papers studying the symmetry of bands, a tight-binding model (TBM) is used. In particular this was done in Ref. [8], where the symmetry classification was done by identifying the bands, obtained in the framework of density-functional-theory (DFT) band-structure calculations [7], with those obtained by applying the group theory algebra to the TBM. However, the band calculations give not only the dispersion law, which was used previously, but also the wave functions. Moreover, in the DFT band structure of a graphene sheet additional information about the nearby environment is contained. Thus in such calculations two free-electron-like lowest-energy conduction bands located at energies below the vacuum level with wave functions spatially largely spread into the vacuum are observed [10–12]. Among these states the lowest-energy band observed experimentally in graphene [13–15] is sharing a common origin with an image-potential state in graphite [11,16,17], a so-called interlayer band in graphite [16,18,19] and intercalated graphite [10,20], image states in nanotubes [21–24], and superatom states in fullerenes [25–27]. Recently these two states were interpreted as being the DFT analogs of two lowest-energy members of a double-Rydberg series of graphene [28].

In the present work, by comparing the results of the TBM and the DFT approaches to the symmetry labeling of the energy bands, we identify the eight bands (four valence and four conducting bands) corresponding to all TBM-derived σ- and π-like energy bands. The identified conduction bands are all lying, completely or partially, inside the vacuum continuum in the vicinity of the Brillouin zone (BZ) center. However, upon approaching the zone boundaries, these bands experience strong hybridization with the free-electron-like states and dramatically change their spatial localization.

II. TIGHT-BINDING MODEL

Partial symmetry analysis of the energy bands in graphene based on group theory algebra in the framework of the TBM was presented in our previous publications [7,8]. This is why in the present work, while briefly mentioning the previously obtained results, we concentrate on the symmetry analysis at point M and lines K-M and Γ-M lacking in our previous publications.

Our TBM space includes four atomic orbitals: $|s,p\rangle$. (Notice that we assume only symmetry of the basis functions with respect to rotations and reflections; the question of how these functions are connected with the atomic functions of the isolated carbon atom is irrelevant.) We look for the solution of the Schrödinger equation as a linear combination of the functions

$$\psi^{j}_{\beta;\mathbf{k}} = \sum_{\mathbf{R}_j} \psi_\beta(\mathbf{r}-\mathbf{R}_j)e^{i\mathbf{k}\cdot\mathbf{R}_j}, \tag{1}$$

*eugene.kogan@biu.ac.il
†nazarov@gate.sinica.edu.tw
‡vyacheslav.silkin@ehu.es
§moshe.kaveh@biu.ac.il

TABLE I. Character table for irreducible representations of the C_s and C_i point groups and the C_{6v}, D_6, and D_{3h} point groups.

C_s	C_i	E	σ	C_{6v}	D_6	D_{3h}	E	C_2	$2C_3$	$2C_6$	$3\sigma_v$	$3\sigma_v'$
		E	I				E	C_2	$2C_3$	$2C_6$	$3U_2$	$3U_2'$
						D_{3h}	E	σ	$2C_3$	$2S_3$	$3U_2$	$3\sigma_v$
A'	A_g	1	1	A_1	A_1	A_1'	1	1	1	1	1	1
A''	A_u	1	−1	A_2	A_2	A_2'	1	1	1	1	−1	−1
				B_2	B_1	A_1''	1	−1	1	−1	1	−1
				B_1	B_2	A_2''	1	−1	1	−1	−1	1
				E_2	E_2	E'	2	2	−1	−1	0	0
				E_1	E_1	E''	2	−2	−1	1	0	0

where ψ_β are atomic orbitals, $j = A,B$ labels the sublattices, and $\mathbf{R}_j$ is the radius vector of an atom in the sublattice j. A symmetry transformation of the functions $\psi^j_{\beta;\mathbf{k}}$ is a direct product of two transformations: the transformation of the sublattice functions $\phi^{A,B}_{\mathbf{k}}$, where

$$\phi^j_{\mathbf{k}} = \sum_{\mathbf{R}_j} e^{i\mathbf{k}\cdot\mathbf{R}_j}, \tag{2}$$

and the transformation of the orbitals ψ_β. Thus the representations realized by the functions (1) will be the direct product of two representations.

The Hamiltonian of graphene being symmetric with respect to reflection in the graphene plane, the bands built from the $|z\rangle$ orbitals decouple from those built from the $|s,x,y\rangle$ orbitals. The former are odd with respect to reflection; the latter are even. In other words, the former form π bands, and the latter form σ bands.

In symmetry analysis it is natural to start from the most symmetrical point Γ. The group of wave vector $\mathbf{k}$ at the Γ point is D_{6h}. We have to admit that in our previous publications [7,8] we made mistakes while connecting representations of group D_{6h} with those of group C_{6v}. This is why this time we present this transition with maximum details in the Appendix. There it is shown that at point Γ, $|z\rangle$ orbitals realize the $A_{2u} + B_{2g}$ representation, $|s\rangle$ orbitals realize the $A_{1g} + B_{1u}$ representation, and $|x,y\rangle$ orbitals realize the $E_{1u} + E_{2g}$ representation of group D_{6h}.

The group of wave vector $\mathbf{k}$ at the K point is D_{3h}. In Ref. [8] it was found that at this point the orbitals $|z\rangle$ realize the E'' representation, the orbitals $|s\rangle$ realize the E' representation, and the orbitals $|x,y\rangle$ realize the $A_1' + A_2' + E'$ representation of group D_{3h}.

The group of wave vector $\mathbf{k}$ at each of the lines constituting triangle Γ-K-M is C_{2v} [29]. Representations realized at the Γ and K points determine unambiguously representations realized at the lines of the triangle.

At the line Γ-K the symmetry operations for group C_{2v} correspond respectively to the symmetry operations for group D_{3h}: C_2-U_2, σ_v-σ, σ_v'-σ_v; and correspond respectively to the symmetry operations for group D_{6h}: C_2-U_2', σ_v-C_2I, σ_v'-U_2I. This correspondence allows one to obtain compatibility between the one-dimensional representations of group D_{6h} (D_{3h}) and the representations of group C_{2v} by inspection.

To obtain the decomposition of the two-dimensional representations of group D_{6h} (D_{3h}) with respect to the representations of group C_{2v} at line Γ-K, it is convenient to use the following equation,

$$a_\alpha = \frac{1}{g}\sum_G \chi(G)\chi^*_\alpha(G), \tag{3}$$

which shows how many times a given irreducible representation α is contained in a reducible one [30]. In Eq. (3) g is the number of elements in the group, $\chi_\alpha(G)$ is the character of an operator G in the irreducible representation α, and $\chi(G)$ is the character of the operator G in the representation being decomposed. Using Tables I and II we obtain the decomposition of the two-dimensional representations of group D_{6h} in the following forms,

$$\begin{aligned} E_{1u} &= A_1 + B_1, \\ E_{2g} &= A_1 + B_1, \end{aligned} \tag{4}$$

and we obtain the decomposition of the two-dimensional representations of group D_{3h} in the following forms,

$$\begin{aligned} E' &= A_1 + B_1, \\ E'' &= A_2 + B_2. \end{aligned} \tag{5}$$

At the line Γ-M the symmetry operations for group C_{2v} correspond, respectively, to the symmetry operations for group D_{6h}: C_2-U_2, σ_v-C_2I, σ_v'-$U_2'I$. This correspondence allows one to obtain compatibility between the one-dimensional representations of group D_{6h} and the representations of group C_{2v} by inspection. Using Eq. (3) we again obtain the decomposition of the two-dimensional representations of group D_{6h} given by Eq. (4).

At the line K-M the symmetry operations for group C_{2v} correspond, respectively, to the symmetry operations for group D_{3h}: C_2-U_2, σ_v-σ, σ_v'-σ_v. This correspondence allows one to obtain compatibility between the one-dimensional representations of group D_{3h} and the representations of group C_{2v} by

TABLE II. Character table for irreducible representations of the C_{2v} and D_2 point groups.

C_{2v}	D_2	E	C_2	σ_v	σ_v'
		E	C_2^z	C_2^y	C_2^x
$A_1; z$	A	1	1	1	1
$B_2; y$	$B_3; x$	1	−1	−1	1
A_2	$B_1; z$	1	1	−1	−1
$B_1; x$	$B_2; y$	1	−1	1	−1

TABLE III. Correlation table of the representations of D_{2h}, which is the point-group symmetry at M, with the representations of C_{2v}, which is the point-group symmetry at the lines of the triangle Γ-K-M.

M	A_g	B_{1g}	B_{2g}	B_{3g}	A_u	B_{1u}	B_{2u}	B_{3u}
Γ-M	A_1	B_1	B_2	A_2	A_2	B_2	B_1	A_1
Γ-(K)-M	A_1	B_1	A_2	B_2	A_2	B_2	A_1	B_1

inspection. Using Eq. (3) we again obtain the decomposition of the two-dimensional representations of group D_{3h} given by Eq. (5).

Now consider the M point. The group of wave vector **k** at this point is D_{2h}. The symmetry analysis of the bands at point M based on the symmetry of the atomic orbitals in the TBM is presented in the Appendix. There it is shown that at point M, $|z\rangle$ orbitals realize the $B_{1u} + B_{2g}$ representation, $|s\rangle$ orbitals realize the $A_g + B_{3u}$ representation, $|x\rangle$ orbitals realize the $A_g + B_{3u}$ representation, and $|y\rangle$ orbitals realize the $B_{2u} + B_{1g}$ representation of group D_{6h}.

However, there is another way to find representations realized at point M, based on the compatibility relations. Of course, the two methods are in agreement with each other. Two groups C_{2v}, one at line Γ-M and another at line K-M, being combined, contain all the symmetry operations of group D_{2h} at point M. Hence representations at lines Γ-M and K-M being taken together unambiguously determine irreducible representations realized at point M. Such correspondence is presented in Table III [29].

In Fig. 1 we present the results of the band-structure calculations with symmetry labeling of the valence and the lowest-lying conduction bands. Additional mathematical details of the bands' symmetry analysis are given in the Appendix. When looking at Fig. 1 (and at Table III) it is important to clearly understand the choice of the Cartesian coordinate systems (which we chose following Ref. [29]). In particular, the principal axis at M is the same as the one at Γ; that is, the z axis is normal to the plane and the x axis is in the direction of point M. The Cartesian coordinate system along the Γ-K and the Γ-M lines differs from the one at the high-symmetry points [29]. Thus the z axis at the Γ-M line is chosen along the Γ-M direction. This explains why, for example, the band which at the Γ-M line realizes representation A_1 and at the K-M line realizes representation B_1, realizes at point M representation B_{3u}.

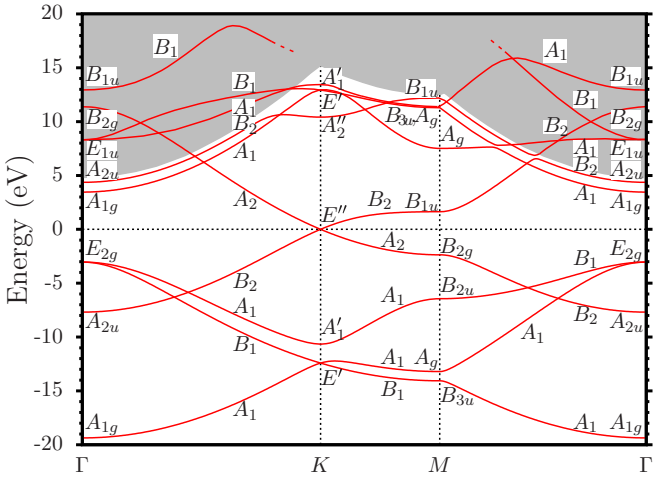

FIG. 1. (Color online) Graphene band structure evaluated with use of the FP-LAPW method and the code ELK [31]. The dashed line shows the Fermi energy.

Now consider the correspondence between the symmetry of the bands given by the TBM and the DFT. The TBM which uses the basis consisting of four orbitals per atom with the given symmetry (plus the given symmetry of the lattice) strongly restricts the possible symmetry of the electron bands. The symmetry of all the bonding (valence) bands and the symmetry of the bands, which realize at the Γ point representations E_{1u}, B_{2g}, and B_{1u} obtained from the DFT (see the next section), correspond to the predictions of the TBM.

Note that it has recently been shown [32] that parts of the bands inside the vacuum continuum (gray background in Fig. 1) turn from true bound-state bands into scattering resonances, by acquiring a finite lifetime due to the coupling of the in-plane and the perpendicular motions. Nevertheless, the current DFT calculation allows us to trace these bands over large portions of the BZ.

III. DFT BAND STRUCTURE

In this section we concentrate first on the two lowest-energy conduction bands, which are not TBM bands. The lowest-energy conduction band has A_{1g} symmetry at the Γ point and A_1 symmetry along the Γ-K line; i.e., it resembles a bonding σ-state A_{1g} as confirmed by its charge-density distribution in the vicinity of the carbon ions presented in Fig. 3 of Ref. [28]. As seen in Fig. 1, this band maintains an almost free-electron-like character over the entire BZ. The next conduction band labeled A_{2u} at the Γ point, B_2 along the Γ-K line, A_2'' at the K point, and B_{1u} at the M point, looks like a π band. Its charge-density distribution around the carbon ions presented at the Γ point in Fig. 3 of Ref. [28] confirms this assignment. This band around the Γ point also has a free-electron-like dispersion in accordance with the location of the majority of its charge on the vacuum side [28]. However, in variance with the lowest-energy conduction band, upon approaching the K point, its dispersion is strongly affected by the interaction with other bands. Thus, charge-density distribution in the A_2'' state is strongly attracted to the graphene sheet with the maximum located at $z \approx 1.5$ a.u. instead of its location at $z \approx 6$ a.u. at the Γ point [11,28]. Moreover, any presence of the π component in the vicinity of the carbon ions is washed out in the A_2'' state. Upon approaching the M point along the K-M line, the wave function of the states in this band (classified as a B_{1u} state at the M point) re-establishes its large diffusion into the vacuum as seen in Fig. 4(c) and the π-like character around the carbon ions, which is a characteristic of this band at the Γ point. The fact that its symmetry is different from that of the three lowest conduction bands can be realized just by looking at the band structure: this band crosses all of them.

Regarding the other unoccupied energy bands, the most simple situation is with the antibonding π band, which is easily identified and disperses upward from the Fermi level up

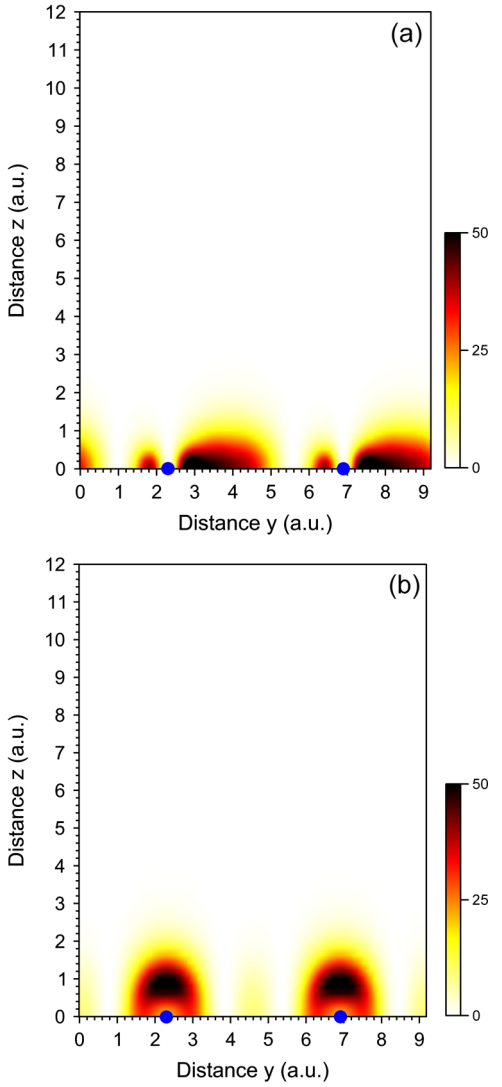

FIG. 2. (Color online) Charge-density distribution (in arbitrary units) in the $y = 0$ plane for (a) E_{1u} and (b) B_{1u} states at the Γ point. Solid dots show the carbon ion positions.

to an energy of $+11.4$ eV. On the other hand, the upper-energy band predicted by the TBM has symmetry B_{1u} at the Γ point and symmetry B_1 along the Γ-K line. The corresponding band can be identified in Fig. 1 as that having an energy of $+13$ eV at Γ. The charge-density distribution in this and one of the E_{1u} states is shown in Fig. 2 where its TBM-like localized character can be easily appreciated.

One of the bands emerging from the double-degenerated E_{1u} state can be traced throughout the whole BZ. Thus in Fig. 1 it is connected to the E' and A_g states at the K and M points, respectively. As one can note in Fig. 3(b), its wave function is distorted from its TBM shape with the significant part located on the vacuum side. On the other hand, this state at the M point still maintains its atomiclike character as seen in Fig. 4(a).

The fate of the second band emanating from the E_{1u} state at finite wave vectors is completely different. Dispersing along the Γ-K line it reaches the K point as an A_1' state with its charge-density distribution presented in Fig. 3(c). Here one can

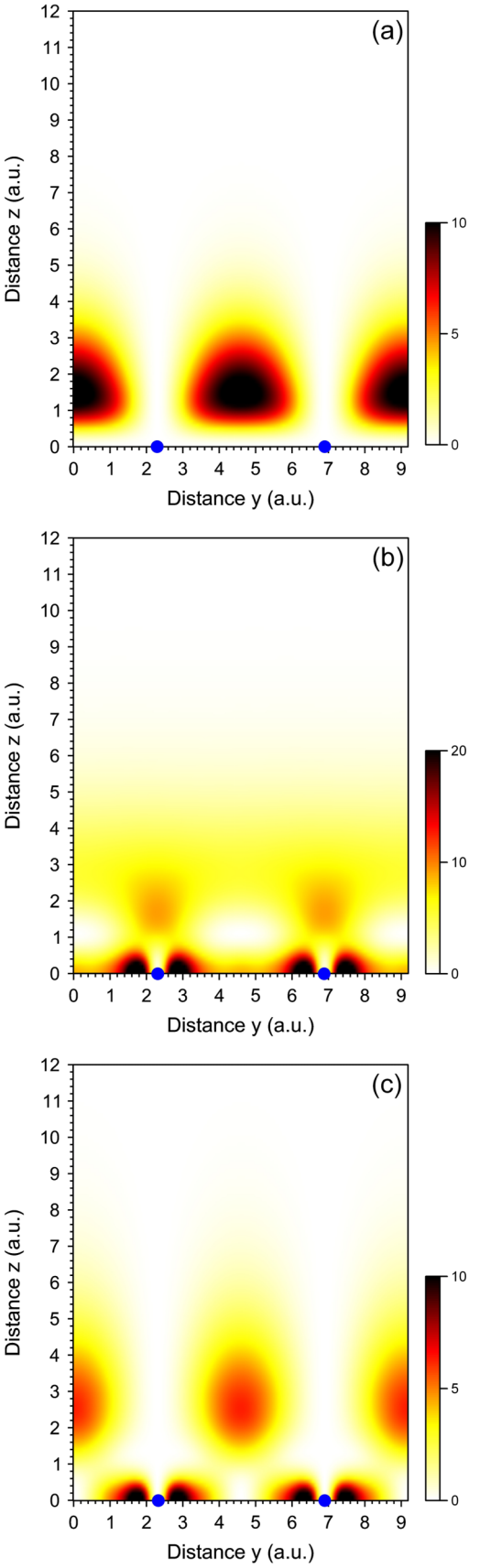

FIG. 3. (Color online) Charge-density distribution (in arbitrary units) in the $y = 0$ plane for (a) A_2'', (b) E', and (c) A_1' states at the K point. Solid dots show the carbon ion positions.

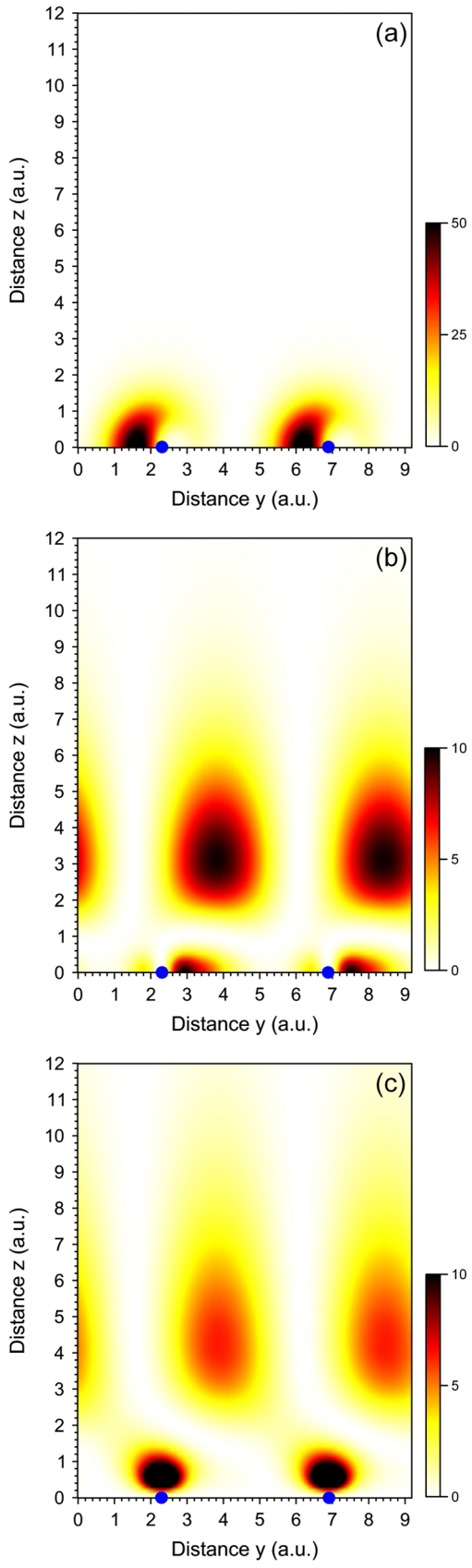

FIG. 4. (Color online) Charge-density distribution (in arbitrary units) in the $y = 0$ plane for (a) lowest-energy unoccupied A_g, (b) B_{3u}, and (c) upper-energy B_{1u} states at the M point. Solid dots show the carbon ion positions.

see that its wave function is even stronger shifted to the vacuum side in comparison with the E' state one. Starting from the Γ point along the Γ-M line this band strongly disperses upward and disappears in the free-electron-like state continuum at energies above ∼17 eV.

The upper atomiclike antibonding state suffers an even stronger hybridization with the vacuum state continuum. The DFT calculation places this band at the Γ point at an energy of 13 eV (a B_{1u} state). As seen in Fig. 2(b), the corresponding charge density has an s-like symmetry in accordance with the TBM prediction [4]. Even being located well-inside the vacuum state continuum this state preserves its atomiclike character in the Γ-point vicinity. In the Γ-M direction this band disperses up to energies of about 16 eV from where its dispersion sharply drops down due to hybridization with the free-electron-like states. The band has at the M point representation B_{3u} characterized by charge-density distribution reported in Fig. 4(b). Its wave function has a strong component on the vacuum side. The dilution of this band within the continuum finds itself in perfect agreement with the theory of scattering resonances in 2D crystals [32], whereas 2D states above the vacuum level decay due to the coupling between the in-plane and the perpendicular motions.

IV. DISCUSSION

One of the aims of the present work was to answer the question: How good is the tight-binding model for graphene? Group theory algebra shows that the assumption that electron wave function can be expanded as a linear combination of four orbitals per atom with the given symmetry, together with the given symmetry of the lattice, unequivocally determines possible representations realized at the symmetry points Γ, K, and M without any additional assumptions about the Hamiltonian. The question is whether these predictions agree with the results of the DFT band calculations. The answer is that they agree partially. More specifically, all four valence bands and three out of the five lowest-lying conduction bands obtained by DFT band calculations correspond to the TBM paradigm.

However, the two lowest-lying (at the Γ point) conduction bands given by the DFT band calculation (one of the σ type and another of the π type) cannot be interpreted in the framework of the TBM. Judging by their symmetry, these bands can be interpreted as plane waves (we mean the wave-function dependence upon the x, y coordinates) orthogonal to the bonding bands. In fact, the lowest energy states built from plane waves will have the maximum symmetry in the plane xy, that is, they will have the same symmetry as the lowest bonding bands in the TBM. Orthogonality of these plane waves to the bonding bands does not change this fact. This is particularly obvious for the non-TBM π^* band, because the plane waves have to be orthogonal to the band of maximum symmetry. The non-TBM σ^* band has to be orthogonal to all three σ valence bands, which, taken together, also have maximum symmetry in the xy plane. And this symmetry is what we see in Fig. 1. The orthogonal plane wave interpretation of the non-TBM bands is supported also by their dispersion law and density distribution (see Figs. 3 and 4).

In our previous publications treating this subject [7,8], we started from the dispersion law given by the DFT calculations and essentially equivalent to that presented on Fig. 1. However, no wave function analysis was performed in the framework of the DFT calculations, and in the symmetry analysis we relied on the group theory exclusively. Thus the assignment of irreducible representations was a delicate process involving compatibility relations and some guesswork.

Now we have to admit that in our previous publications [7,8] there were mistakes in labeling the bands. First, we messed up with the group algebra and wrongly connected representations of group D_{6h} with those of group C_{6v}. This is why this time we present this transition with maximum detail.

Second, it is natural to expect that at point Γ the valence bands are symmetrical with respect to rotation in the plane of graphene by an angle π about the center of the line connecting the two atoms. Such a symmetrical combination is said to be bonding [33]. The conduction bands are antisymmetrical with respect to the rotation (antibonding). If we take into account the symmetry of the $|s,x,y\rangle$ orbitals and the antisymmetry of the $|z\rangle$ orbitals with respect to reflection in the plane, we come to the conclusion that valence σ bands at point Γ should correspond to even representations (index g), and the valence π band should correspond to odd representations (index u) [4]. In our previous publications [7,8] we have ignored this fact while assigning representations to the $|x,y\rangle$ bands at point Γ.

A quantitative argument supporting the correct assignment was communicated to us by an anonymous referee. In the TBM with the nearest neighbor coupling at the Γ point neglecting overlaps we get

$$E(E_{2g}) - E(E_{1u}) = -3[H_{pp\sigma} + H_{pp\pi}] \tag{6}$$

(see Ref. [34] for notation). Using the values for the couplings [34,35] $H_{pp\sigma} = 5.1$ eV and $H_{pp\pi} = -3.1$ eV, we obtain

$$E(E_{2g}) - E(E_{1u}) = -6 \text{ eV}, \tag{7}$$

which means that the E_{2g} representation characterizes the valence band at point Γ and the E_{1u} representation characterizes the conduction band. Of course, this assignment is proven by analysis of the wave function obtained in the framework of the DFT, which we did.

By analyzing the band structure we have discovered empirically an unexpected topological classification of the bands. There are bands for which the energy returns to itself when the wave vector changes continuously along the closed curve Γ-K-M-Γ. There are also bands where, to return to the same value of energy, the wave vector has to traverse the curve two or even three times (see Fig. 1). The more detailed analysis of this classification will be the subject of a separate publication.

Finally, we would like to emphasize that the present paper corrects and extends previous work by some of its authors [7,8]. The main new contributions are the following.

(i) The symmetry classification of energy bands is extended to include the M point and the adjoining lines K-M and Γ-M (Fig. 1).

(ii) Some previous assignments of irreducible representations are corrected, including those of the two lowest-energy conduction bands (Fig. 1 and Sec. III).

(iii) The charge-density distributions of some states are presented and discussed (Sec. III and Figs. 2–4).

ACKNOWLEDGMENTS

Discussions with E. E. Krasovskii, which were very helpful to us, are gratefully acknowledged. V.U.N. acknowledges support from the National Science Council, Taiwan (Grant No. 100-2112-M-001-025-MY3). We owe a lot to the anonymous referee, whose comments actually corrected several serious mistakes in the initial version of the present paper.

APPENDIX

Consider the symmetry analysis at the Γ point. The group of the wave vector is D_{6h}. In Ref. [8] representations of group D_{6h} were obtained on the basis of the identity

$$D_{6h} = C_{6v} \times C_s. \tag{A1}$$

It was found that the functions $\psi^j_{z;\mathbf{0}}$ realize the

$$(A_1 + B_2) \times A'' \tag{A2}$$

representation, the functions $\psi^j_{s;\mathbf{0}}$ realize the

$$(A_1 + B_2) \times A' \tag{A3}$$

representation, and the functions $\psi^j_{x,y;\mathbf{0}}$ realize the

$$(E_1 + E_2) \times A' \tag{A4}$$

representation of group D_{6h}. In Eqs. (A2)–(A4) the first multiplier refers to the irreducible representations of group C_{6v}, and the second multiplier refers to the irreducible representations of group C_s (the character tables are presented in Table IV).

However, the irreducible representations of group D_{6h} are traditionally labeled not on the basis of the identity (A1), but on the basis of the alternative identity

$$D_{6h} = D_6 \times C_i. \tag{A5}$$

Thus each representation of group D_6, say A_1, begets two representations: even A_{1g} and odd A_{1u}.

To decompose the product of representations (A2)–(A4) with respect to the irreducible representations of group D_{6h} we need to express the products of the symmetry operations of groups C_{6v} and C_s through the products of the symmetry operations of groups D_6 and C_i. Using elementary algebra

TABLE IV. Correspondence between the products of the symmetry operations of groups D_6 and C_i and the products of the symmetry operations of groups C_{6v} and C_s.

E	C_2	C_3	C_6	U_2	U_2'	I	C_2I	C_3I	C_6I	U_2I	$U_2'I$
E	C_2	C_3	C_6	$\sigma_v\sigma$	$\sigma_v'\sigma$	$C_2\sigma$	σ	$C_6\sigma$	$C_3\sigma$	σ_v'	σ_v

we obtain

$$\begin{aligned} A_1 \times A' &= A_{1g}, \\ B_2 \times A' &= B_{1u}, \\ A_1 \times A'' &= A_{2u}, \\ B_2 \times A'' &= B_{2g}, \\ E_1 \times A' &= E_{1u}, \\ E_2 \times A' &= E_{2g}. \end{aligned} \tag{A6}$$

All the representations in the right-hand side of Eq. (A6) are realized at point Γ.

Now consider point M. The group of wave vector $\mathbf{k}$ at the point is D_{2h}. Irreducible representations of point group D_{2h} are obtained on the basis of identity:

$$D_{2h} = D_2 \times C_i. \tag{A7}$$

As is obvious from Table II, the $|z\rangle$ orbitals realize the B_{1u} representation, the $|s\rangle$ orbitals realize the A_g representation, the $|x\rangle$ orbitals realize the B_{3u} representation, and the $|y\rangle$ orbitals realize the B_{2u} representation of group D_{2h} [We are considering $M = (\frac{2\pi}{3a},0)$]. For the basis $\phi^j_{\mathbf{M}}$, we get $\chi(E) = \chi(IC_z) = \chi(C_x) = \chi(IC_y) = 2$. The characters corresponding to other transformations are equal to zero. Hence the functions $\phi^j_{\mathbf{M}}$ realize the $A_g + B_{3u}$ representation of group D_{2h}. Using elementary algebra we obtain

$$\begin{aligned} B_{1u} \times A_g &= B_{1u}, \\ B_{1u} \times B_{3u} &= B_{2g}, \\ A_g \times A_g &= A_g, \\ A_g \times B_{3u} &= B_{3u}, \\ B_{3u} \times A_g &= B_{3u}, \\ B_{3u} \times B_{3u} &= A_g, \\ B_{2u} \times A_g &= B_{2u}, \\ B_{2u} \times B_{3u} &= B_{1g}. \end{aligned} \tag{A8}$$

All the representations in the right-hand side of Eq. (A8) but one are realized at point M. The missing B_{1g} representation would certainly correspond to the highest TBM band (see Table III) were we are able to follow the band to point M.

[1] W. M. Lomer, Proc. R. Soc. London, Ser. A **227**, 330 (1955).
[2] J. C. Slonczewski and P. R. Weiss, Phys. Rev. **109**, 272 (1958).
[3] G. Dresselhaus and M. S. Dresselhaus, Phys. Rev. **140**, A401 (1965).
[4] F. Bassani and G. Pastori Parravicini, Nuovo Cimento B **50**, 95 (1967).
[5] L. M. Malard, M. H. D. Guimaraes, D. L. Mafra, M. S. C. Mazzoni, and A. Jorio, Phys. Rev. B **79**, 125426 (2009).
[6] J. L. Manes, Phys. Rev. B **85**, 155118 (2012).
[7] E. Kogan and V. U. Nazarov, Phys. Rev. B **85**, 115418 (2012).
[8] E. Kogan, Graphene **2**, 74 (2013).
[9] W. J. Elder, E. S. Tok, D. D. Vvedensky, and J. Zhang, arXiv:1306.2520.
[10] M. Posternak, A. Baldereschi, A. J. Freeman, E. Wimmer, and M. Weinert, Phys. Rev. Lett. **50**, 761 (1983).
[11] M. Posternak, A. Baldereschi, A. J. Freeman, and E. Wimmer, Phys. Rev. Lett. **52**, 863 (1984).
[12] T. O. Wehling, I. Grigorenko, A. I. Lichtenstein, and A. V. Balatsky, Phys. Rev. Lett. **101**, 216803 (2008).
[13] D. Pacilé, M. Papagno, A. Fraile Rodríguez, M. Grioni, L. Papagno, Ç. Ö. Girit, J. C. Meyer, G. E. Begtrup, and A. Zettl, Phys. Rev. Lett. **101**, 066806 (2008).
[14] D. Niesner, T. Fauster, J. I. Dadap, N. Zaki, K. R. Knox, P.-C. Yeh, R. Bhandari, R. M. Osgood, M. Petrović, and M. Kralj, Phys. Rev. B **85**, 081402(R) (2012).
[15] N. Armbrust, J. Güdde, P. Jakob, and U. Höfer, Phys. Rev. Lett. **108**, 056801 (2012).
[16] Th. Fauster, F. J. Himpsel, J. E. Fischer, and E. W. Plummer, Phys. Rev. Lett. **51**, 430 (1983).
[17] S. Pagliara, M. Montagnese, S. Dal Conte, G. Galimberti, G. Ferrini, and F. Parmigiani, Phys. Rev. B **87**, 045427 (2013).
[18] N. A. W. Holzwarth, S. G. Louie, and S. Rabii, Phys. Rev. B **26**, 5382 (1982).
[19] V. N. Strocov, P. Blaha, H. I. Starnberg, M. Rohlfing, R. Claessen, J.-M. Debever, and J.-M. Themlin, Phys. Rev. B **61**, 4994 (2000).
[20] G. Csányi, P. B. Littlewood, A. H. Nevidomskyy, C. J. Pickard, and B. D. Simons, Nat. Phys. **1**, 42 (2005).
[21] K. Schouteden, A. Volodin, D. A. Muzychenko, M. P. Chowdhury, A. Fonseca, J. B. Nagy, and C. Van Haesendonck, Nanotechnology **21**, 485401 (2010).
[22] B. E. Granger, P. Král, H. R. Sadeghpour, and M. Shapiro, Phys. Rev. Lett. **89**, 135506 (2002).
[23] M. Zamkov, N. Woody, B. Shan, H. S. Chakraborty, Z. Chang, U. Thumm, and P. Richard, Phys. Rev. Lett. **93**, 156803 (2004).
[24] S. L. Hu, J. Zhao, Y. D. Jin, J. L. Yang, H. Petek, and J. G. Hou, Nano Lett. **10**, 4830 (2010).
[25] M. Feng, J. Zhao, and H. Petek, Science **320**, 359 (2008).
[26] H. Petek and J. Zhao, Chem. Rev. **110**, 7082 (2010).
[27] G. J. Dutton, D. B. Dougherty, W. Jin, J. E. Reutt-Robey, and S. W. Robey, Phys. Rev. B **84**, 195435 (2011).
[28] V. M. Silkin, J. Zhao, F. Guinea, E. V. Chulkov, P. M. Echenique, and H. Petek, Phys. Rev. B **80**, 121408(R) (2009).
[29] C. Thomsen, S. Reich, and J. Maultzsch, *Carbon Nanotubes: Basic Concepts and Physical Properties* (Wiley Online Library, Wiley-VCH Verlag GmbH, 2004).
[30] L. D. Landau and E. M. Lifshitz, *Quantum Mechanics*, Course of Theoretical Physics Vol. 3 (Pergamon, Elmsford, NY, 1991).
[31] http://elk.sourceforge.net
[32] V. U. Nazarov, E. E. Krasovskii, and V. M. Silkin, Phys. Rev. B **87**, 041405 (2013).
[33] C. Kittel, *Quantum Theory of Solids* (Wiley & Sons, New York/London, 1963).
[34] B. Gharekhanlou and S. Khorasani, in *Graphene: Properties, Synthesis and Applications*, edited by Zhiping Xu (Nova Science Publishers, New York, 2011).
[35] R. Saito, G. Dresselhaus, and M. S. Dresselhaus, *Physical Properties of Carbon Nanotubes* (Imperial, London, 1998).